

Thermal Evolution near Heat-Generating Nuclear Waste Canisters Disposed in Horizontal Drillholes

Published in *Energies*, 12(4), 596, doi:10.3390/en12040596; February 13, 2019.

AUTHORED BY:

Stefan Finsterle
Richard A. Muller
Rod Baltzer
Joe Payer
James W. Rector



Article

Thermal Evolution near Heat-Generating Nuclear Waste Canisters Disposed in Horizontal Drillholes

Stefan Finsterle ^{1,*}, Richard A. Muller ², Rod Baltzer ², Joe Payer ³ and James W. Rector ⁴

¹ Finsterle GeoConsulting; 315 Vassar Ave, Kensington, CA 94708, USA

² Deep Isolation Inc., 2120 University Ave, Suite 623, Berkeley, CA 94704, USA; rich@deepisolation.com (R.A.M.); rod@deepisolation.com (R.B.)

³ Corrosion Engineering, University of Akron, Whitby Hall 211, Akron, OH 44325, USA; jpayer@uakron.edu

⁴ Department of Civil and Environmental Engineering, University of California; Berkeley, CA 94720, USA; jwrector@berkeley.edu

* Correspondence: stefan@finsterle-geoconsulting.com; Tel.: +1-510-516-2506

Received: 21 December 2018; Accepted: 11 February 2019; Published: 13 February 2019



Abstract: We consider the disposal of spent nuclear fuel and high-level radioactive waste in horizontal holes drilled into deep, low-permeable geologic formations using directional drilling technology. Residual decay heat emanating from these waste forms leads to temperature increases within the drillhole and the surrounding host rock. The spacing of waste canisters and the configuration of the various barrier components within the horizontal drillhole can be designed such that the maximum temperatures remain below limits that are set for each element of the engineered and natural repository system. We present design calculations that examine the thermal evolution around heat-generating waste for a wide range of material properties and disposal configurations. Moreover, we evaluate alternative layouts of a monitoring system to be part of an in situ heater test that helps determine the thermal properties of the as-built repository system. A data-worth analysis is performed to ensure that sufficient information will be collected during the heater test so that subsequent model predictions of the thermal evolution around horizontal deposition holes will reliably estimate the maximum temperatures in the drillhole. The simulations demonstrate that the proposed drillhole disposal strategy can be flexibly designed to ensure dissipation of the heat generated by decaying nuclear waste. Moreover, an in situ heater test can provide the relevant data needed to develop a reliable prediction model of repository performance under as-built conditions.

Keywords: nuclear waste isolation; horizontal disposal drillholes; thermal period; design calculations; in situ heater test; data-worth analysis; iTOUGH2

1. Introduction

We examine the geologic disposal of spent nuclear fuel (SNF) and high-level radioactive waste (HLW) using corrosion-resistant canisters placed in deep, sub-horizontal, small-diameter holes drilled in suitable hydrostratigraphic units that safely and securely isolate the waste from the accessible environment. The horizontal drillhole disposal concept takes advantage of the directional drilling experience gained by the oil and gas industry. A vertical access hole cased with a steel pipe is drilled, preferably at or near the site where the nuclear waste is currently stored in surface facilities. At the kickoff point (slightly above the targeted repository depth), the drillhole gradually curves until it is nearly horizontal, with a slight upward tilt. The diameter of the drillhole varies from 9 to 30 inches (0.23 to 0.76 m) depending on the waste type and canister dimensions. Canisters containing the waste are lowered into the vertical access hole and pushed into the horizontal disposal section; they are emplaced end-to-end (potentially spaced apart by a separation distance that is one of the design

parameters investigated in the current analysis) in a casing that lines the drillhole. The disposal section and vertical access hole are eventually sealed. Additional information about the concept can be found on the technology page of Reference [1].

As for any other geologic disposal concept (such as mined repositories or deep vertical borehole disposal), the performance of the engineered and natural barrier systems must be assessed for the specific repository design and the conditions expected during the regulatory compliance period. We focus here on the thermal aspects of such an assessment and how they impact design decisions.

Nuclear waste releases heat due to the decay of radionuclides, elevating temperatures within the canister. The heat then dissipates into the nearby engineered structures and the host formation. Predicting the temperature evolution within the disposal section of the drillhole and the surrounding host rock is necessary as it may alter the properties of the multi-barrier system by accelerating the corrosion of the waste form [2,3] and of metal components comprising the containment systems [4–6], by degrading bentonite [7–9] or cement [10] used as backfill materials, and by affecting argillaceous host rocks [11,12]. Heat-driven degradation mechanisms may also make the retrievability of the waste canisters more difficult. Furthermore, temperature variations may lead to driving forces that affect the migration of radionuclides in the near field of the repository. The maximum allowable temperature—which needs to be determined by analysing the acceptable impact on barrier functions, and which may eventually be set by the regulator—is thus an important design variable for a geological repository, because it determines interim storage time as well as canister loading, canister spacing, and the minimum distance between disposal drillholes. All these factors affect the configuration and length, and thus cost, of the drillholes for a given amount of waste.

The decay heat is time-dependent and determined by (a) the radionuclide inventory of the waste (itself a function of waste type and, in the case of SNF, initial enrichment and burnup percentage) and (b) the duration of post-reactor cooling. The initial temperature rise and subsequent cooling period are referred to as the heat pulse, which typically lasts a few decades to a few hundred years, until temperatures approach their ambient values prior to waste emplacement.

The temperature evolution during the heat pulse has been extensively studied for various disposal systems using both laboratory and field experiments as well as numerical analyses. Large-scale, long-term heater tests for mined repositories in the saturated zone have been conducted in underground rock laboratories dedicated to nuclear waste research [13–15]. Data collected during these experiments were analysed using advanced simulators to predict and reproduce the observed thermal, hydrological, geomechanical, and geochemical evolution of various buffer materials and the surrounding formation [14–20]. These studies reveal the importance of heat generation as it induces coupled thermal-hydrologic (TH) effects. Strong thermal perturbations also affect the geochemical conditions as well as the geomechanical properties and stress state of the repository components, with complex feedback mechanisms to thermal and hydrologic processes. Several heater tests were also conducted and numerically analysed as part of the Yucca Mountain project [21–27]. The unsaturated, highly fractured volcanic rocks at Yucca Mountain and the arrangement of waste packages in open disposal drifts leads to conditions that are significantly different from those encountered in repositories that emplace waste in backfilled deposition holes located in the saturated zone. Since the latter configuration is more akin to that encountered in deep horizontal drillhole disposal, thermal testing and modelling at Yucca Mountain are not discussed further here. Finally, the thermal effects arising from the disposal of high-level radioactive waste in vertical boreholes drilled deep into crystalline basement rocks of the continental crust were investigated using semi-analytical and numerical models [28–30]. Some of these analyses also examined fluid flow induced by the thermal expansion of the rocks and the pore fluids, and considered very high temperatures designed to partially melt and recrystallize the granitic host rock for additional borehole sealing [31,32].

The concept of disposing nuclear waste in horizontal drillholes has some favourable attributes. In addition to operational advantages, there are a number of beneficial factors. For example, the reducing environment of a fully saturated host rock further prolongs the longevity of the canisters

that are made of corrosion-resistant alloy. The linear arrangement of heat-generating nuclear waste in a drillhole makes thermal management considerably less challenging, as will be discussed below. Boiling of water at depth can be avoided, reducing the complexities of multi-phase flow processes. Moreover, relatively minor temperature changes lead to weaker thermal-mechanical stresses, helping to preserve the integrity of the engineered barriers and reducing the disturbance to the host formation. These attributes considerably reduce uncertainties that need to be propagated through performance assessment calculations and strengthen the technical basis for the safety case.

The goal of the present analysis is to examine the impact of (a) design parameters and (b) uncertainty in host-rock thermal properties on temperatures in and around a horizontal disposal drillhole. Response surfaces are generated based on numerical simulations of heat dissipation in such a system. Moreover, sensitivity and data-worth analyses are performed to help design an in situ heater experiment that can reduce the uncertainty in subsequent model predictions.

The analyses show that the temperature evolution in a horizontal drillhole containing heat-generating nuclear waste can be managed by adjusting a few design parameters. The thermal properties of the host formation have a dominant influence on the temperature evolution; these properties thus must be determined with sufficiently low estimation uncertainty, which can be accomplished by appropriate drillhole characterization methods and the collection of sensitive data during a short-term heater test.

2. Conceptual and Numerical Model Development

Waste emplacement geometry and configuration of the engineered barriers within the horizontal drillhole need to be designed such that the maximum temperatures remain below limits that are set for each component of the engineered and natural repository system. The design calculations presented below are based on numerical simulations. The sophistication of the conceptual model to be developed and the level of detail with which features and processes must be represented are given by the specific purpose of the model, which in this case is to examine the thermal evolution around heat-generating waste canisters for a wide range of material properties and disposal configurations. Such scoping calculations typically have lower requirements regarding fidelity and accuracy than detailed studies in support of the safety case and performance assessment for a nuclear waste repository. Nevertheless, the simplifying assumptions made during model development must be transparent and justified in the context of the ultimate analysis to be done once the fully detailed configuration is known. The assumptions and model choices made for the current general design calculations are described in the following subsections.

2.1. System Description

The deep horizontal drillhole disposal concept targets a variety of waste forms, ranging from nuclear waste from the U.S. defense program to SNF assemblies from different reactor types to vitrified HLW. While design calculations must accommodate the specifics of each waste type (especially canister geometry and heat output characteristics), the method described here is general and thus, can be illustrated using a single waste type. We consider the disposal of capsules that contain primarily short-lived cesium-137 (^{137}Cs) and strontium-90 (^{90}Sr) [33] extracted in the form of cesium chloride (CsCl) and strontium fluoride (SrF_2) during the chemical processing of defense fuel. The capsules, fabricated from 316L stainless steel, are typically 20.775 inches (0.528 m) long, 2.6 inches (0.066 m) in diameter and weigh less than 10 kg [34,35]. Currently, there are 1335 cesium and 601 strontium capsules stored underwater at the Hanford Waste Encapsulation and Storage Facility; we will study the thermal response to the disposal of these capsules in deep horizontal drillholes.

We propose to insert one or several of such capsules into a canister made of a corrosion-resistant alloy (e.g., Alloy 625); the canister will have an outer diameter of approximately 4.5 inches (0.114 m). The space between the capsule and canister is filled with an appropriate backfill material (such as quartz sand) for mechanical stability and to provide sufficient conductivity for heat dissipation.

The canister is placed in a liner or casing, which has an inner diameter of 5.5 inches (0.140 m). The space between the canister and the casing (and axially between individual canisters) may be filled with drilling fluid, a slurry or a suitable buffer material (such as bentonite). The casing is likely to be cemented into an 8.5 inch (0.216 m) diameter, horizontal drillhole, which is the disposal section of the repository. The disposal section is completed in a host rock that not only exhibits favorable hydrogeological, geochemical and geomechanical properties, but is also protected by low-permeable overlying strata (such as shales, claystones and mudstones) and has been isolated from surface waters and aquifers for very long times, as demonstrated, for example, by isotopic age determination of the resident brines. While drilling may damage the rock around the hole, the thickness of such a skin or excavation disturbed zone is expected to be small with minor impacts on the rock’s thermal properties. It is further assumed that the various components are perfect cylindrical shells that are centered on the drillhole axis. The impact of an off-centered configuration on the temperature distribution has been examined and was determined to be insignificant for the purpose of these scoping calculations.

Figure 1 shows a schematic of the various components in a vertical cross section along and perpendicular to the drillhole axis. We assume that waste capsule spacing is constant, that the heat source is distributed uniformly among and within waste capsules, and that gravity effects can be ignored in and around the horizontal drillhole. Under these conditions, a two-dimensional, radial model can be developed with symmetry planes perpendicular to the drillhole axis at the center of a capsule and at the midpoint between two capsules (see Figure 1c). The capsule spacing is an adjustable design parameter. The outer model radius is large enough to avoid boundary effects.

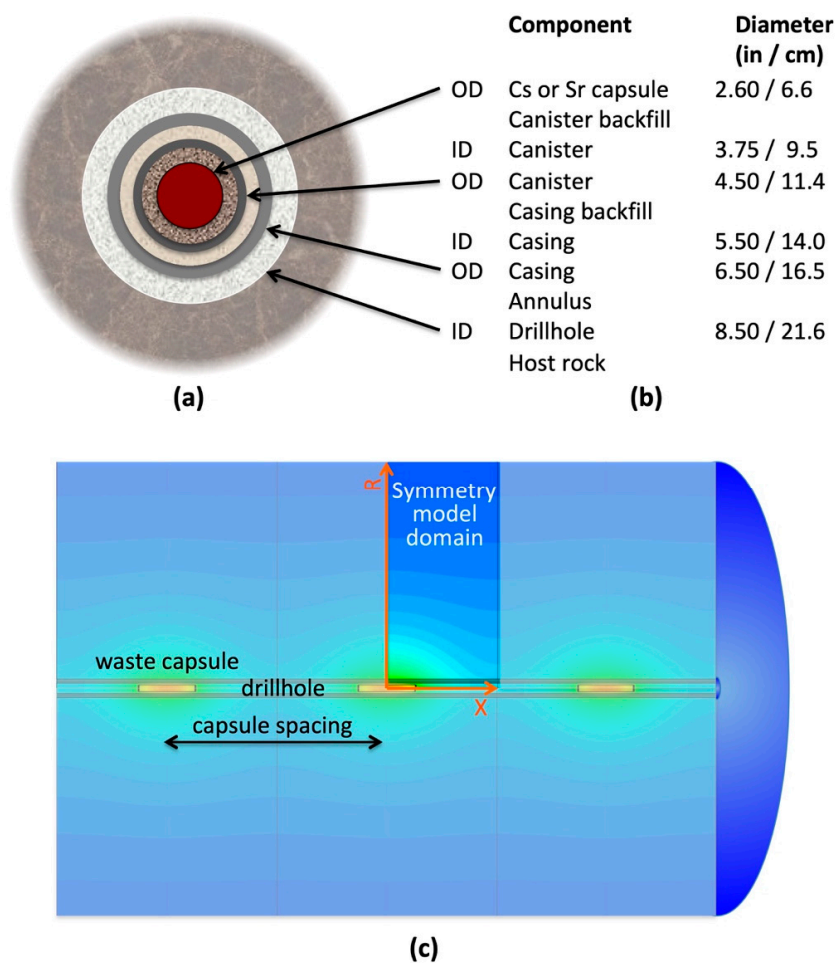


Figure 1. (a) Cross-sectional schematic of components in a horizontal drillhole used for the disposal of heat-generating cesium or strontium capsules; (b) list of inner diameters (ID) and outer diameters (OD) of each component; (c) X-R cross section, showing symmetric model domain.

The average power output (as of 29 August 2007) of a Sr and Cs capsule is 193.2 W and 143.6 W, respectively [34]. The heat output from Sr capsules is substantially more variable than that of Cs capsules, with standard deviations of 101.0 W and 14.1 W, and a maximum output of 504.6 W and 195.4 W, respectively [34]. Nevertheless, the resulting temperature evolution for conduction-dominated heat transfer depends approximately linearly on the heat output, i.e., results calculated for a reference heat generation rate of 100 W per capsule can readily be scaled to capsules with a different initial radioactivity and different cooling period.

As heat generation is directly related to radioactive decay, the time-dependent rate follows the exponential decay curve of the respective isotope, i.e.,

$$Q_H(t) = Q_{H0} \cdot e^{-\lambda_\kappa t}, \quad (1)$$

where Q_{H0} is the initial heat generation rate; λ_κ is the decay constant of isotope κ , which is related to the half-life $T_{1/2}$ by $\lambda_\kappa = (\ln 2)/T_{1/2}$; and t is time. The half-lives of cesium and strontium are, respectively, 30.17 and 28.79 years.

Heat generation will be assigned exclusively to the capsule itself, i.e., no heating of the other components of the drillhole or the host rock due to radiation is considered. This is justified by the fact that ^{90}Sr (and its decay products) undergoes a beta-decay, whereby the emitted electron is absorbed within the capsule. For ^{137}Cs , about 22% of the decay energy is released by short-range electrons; the remaining 78% of the energy released by gamma rays is effectively attenuated in CsCl and Alloy 625, with only a very small fraction being deposited in the casing and virtually none in the host rock.

2.2. Physical Processes

The dissipation of thermal energy in engineered and natural materials is mainly driven by heat conduction, and to a much smaller degree through convection by moving fluids (liquids or gases) and radiative heat transport. Latent heat effects during phase transitions and contributions from changes in the gravitational potential energy [36] also impact the temperature distribution. Many thermal and hydrological processes are strongly coupled, specifically if phase changes occur. Mechanical effects are triggered by thermal stresses, and the geochemistry of pore fluids and the mineral composition of the rocks are affected by temperature. While feedback mechanisms that affect temperature due to chemical reactions and stress changes do exist, they are typically much weaker than coupled thermal-hydrological effects [37]. It can be generally observed that many geochemical or corrosion models require thermal input, whereas thermal calculations rarely require geochemical input. Similarly, most stress calculations require thermal input, whereas thermal calculations rarely require geomechanical input. It is therefore sensible to start the analysis of a novel disposal concept by examining the thermal response to the emplacement of heat-generating waste.

For the deep horizontal drillhole system of interest, conduction is the dominant heat transfer mechanism. This is undoubtedly the case for the hydraulically impermeable, but thermally highly conductive metals of the engineered barrier system, but also for the porous backfill materials and the host rock, which, by design, are of low permeability and porosity and are located in a low hydraulic gradient environment. Radiative heat transfer is negligible for the expected temperatures and in the absence of large open space, or is included in the experimentally determined thermal conductivity value. The gravitational potential energy is irrelevant in the horizontal disposal section of the drillhole, and of no significance in the vertical section, specifically in the absence of fluid flow.

Latent heat effects are not expected in a deep drillhole repository, where ambient fluid pressures are close to hydrostatic and thus likely above the saturated vapor pressure, preventing boiling even for relatively high temperatures. Figure 2 shows the boiling temperature as a function of pressure, which is correlated to depth assuming a hydrostatic pressure profile. For example, for a repository depth of 1 km, temperatures below 300 °C will not lead to boiling. Finally, latent heat effects due to melting and recrystallization of the host rock are not relevant for the temperature range considered in this study.

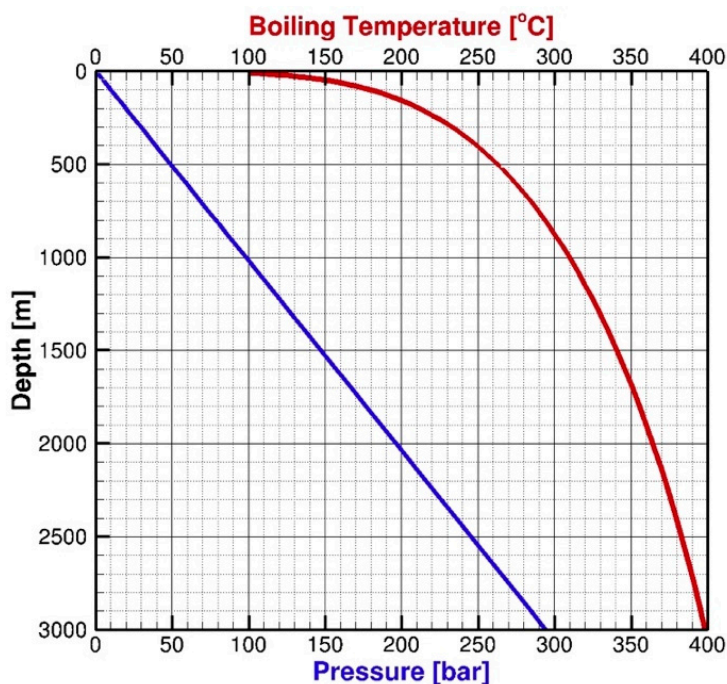


Figure 2. Boiling temperature as a function of pressure and approximate depth, assuming a hydrostatic pressure profile and fully liquid-saturated conditions in the disposal section of the horizontal drillhole.

To avoid the complexity of coupled thermal-hydrological-geochemical processes, which are exacerbated if a steam phase evolves, it is recommended that the maximum allowable temperature in the repository be below the boiling temperature curve shown in Figure 2. Note that a lower maximum temperature criterion may be advisable for other reasons, such as expansion and associated thermal stresses [18] or undesirable mineralogical alterations of the buffer material or host rock [7–9]. Avoiding steam also improves the corrosion performance of engineered barrier components, particularly that of canister materials.

Having heat conduction identified as the dominant heat transfer mechanism, it is essential that the material properties appearing as coefficients in the heat conduction equation are known with an acceptable level of uncertainty, as they are likely the most influential parameters for temperature predictions. Heat conduction is a diffusive process governed by a parameter group referred to as thermal diffusivity, $(K/\rho c)$, where K is the thermal conductivity, ρ is the density, and c is the specific heat. It is important to realize that these are all effective parameters for the bulk material, which consists of multiple components and phases. While density and specific heat can be calculated reasonably well as the volume average of each of the material's components, the thermal conductivity of a composite porous medium depends to a large degree on the connectivity between its more conductive and more resistive components [38,39]. The arrangement and contact of particles and the connectivity of fluids in the pore space of a backfill material or geologic formation is complex and prevents an easy calculation of thermal conductivity from the properties of its components, resulting in a considerable range of values even for similar rock types. Nevertheless, effective thermal conductivities can be experimentally determined with good accuracy. The parameters are also temperature dependent [40,41], with generally decreasing thermal conductivity and increasing heat capacity as temperature increases, partially compensating each other's influence on thermal diffusivity and thus, the overall effect on temperature. For the design calculations discussed below, thermal conductivity is isotropic and constant, and good thermal contact is assumed at material interfaces. Note that even a small gap between two materials (filled by a liquid or gas) has the effect of a relative insulator, which can either be modeled explicitly or accounted for by adjusting the effective thermal conductivity.

The thermal properties of water are well known and only weakly dependent on salinity. Should a special drilling fluid, mud, or slurry be used, their thermal (and hydraulic) properties need to be measured and included in the simulations, specifically if no porous backfill material is used or convection within the drillhole or in the formation becomes significant.

While fluid flow and associated heat conduction is expected to be a minor contributor to heat transfer, it will be accounted for in the simulations. However, it is assumed that the sole driving force for fluid flow is that triggered by the thermal expansion of the fluids and pore space. Note that thermal pore expansivity partly compensates for fluid expansion, and the resulting pressure change is further mediated by elastic deformation of the pores, which in the model is assumed to depend on the pore pressure rather than effective stress.

As discussed above, a time-dependent heat source is specified, which follows the decay curve of the radionuclides in the waste. The heat source is assumed to be uniformly distributed within the volume representing the waste capsule. While the waste is not necessarily uniform, the high thermal conductivity of the capsule is likely to homogenize the temperatures and heat release to the engineered barrier system.

It should be noted that while the heat-driven coupled processes outlined above are inherently complex, the horizontal drillhole concept, which promotes heat dissipation, reduces the thermal stresses and thus the challenge to predict their impacts on repository performance.

2.3. Mathematical and Numerical Model

A mathematical model of the physical processes discussed in the previous subsection is implemented in the TOUGH2 [42] numerical simulator, which calculates non-isothermal, multiphase, multicomponent fluid flow in fractured porous media. TOUGH2 solves mass- and energy-balance equations formulated in a general, integral form. A simplified version (assuming single-phase liquid conditions with water being the only component) of the time-dependent energy balance equation can be written for an arbitrary subdomain V_n , which is delimited by the closed surface Γ_n as [42]

$$\frac{d}{dt} \int_{V_n} [(1 - \phi)\rho_s c_s T + \phi \rho_w u_w] dV_n = \int_{\Gamma_n} [-K \nabla T + h \mathbf{F}] \cdot \mathbf{n} d\Gamma_n + \int_{V_n} q dV_n. \quad (2)$$

The energy accumulation during time interval dt on the left-hand side of Equation (2) contains contributions from the solid and liquid phases, where ϕ is porosity; ρ_s and ρ_w are, respectively, the grain and water densities; T is temperature; c_s is the solid specific heat; and u_w is the specific internal energy of liquid water. The first term on the right-hand side is the heat flux across the volume boundary, which includes conductive and convective components. Here, K is the effective thermal conductivity discussed above, h is the specific enthalpy of liquid water, and \mathbf{n} is a normal vector on the surface element $d\Gamma_n$, pointing inward into V_n . The specific source term q is proportional to the time-dependent decay heat curve of Equation (1). The liquid mass flux \mathbf{F} is given by Darcy's law,

$$\mathbf{F} = \rho_w \mathbf{u} = -k \frac{\rho_w}{\mu_w} (\nabla P - \rho_w \mathbf{g}), \quad (3)$$

where \mathbf{u} is the Darcy velocity, k is absolute permeability, μ_w is the dynamic viscosity of liquid water, P is fluid pressure, and \mathbf{g} is the vector of gravitational acceleration. All thermophysical fluid properties are a function of pressure and temperature, accurately calculated based on the IAPWS-95 formulation [43].

TOUGH2 uses a finite volume formulation for space discretization and a first-order implicit scheme for time discretization. The resulting coupled, nonlinear algebraic equations (with pressure and temperature in each grid block as the unknown primary variables) are solved simultaneously using Newton–Raphson iterations. The elements of the Jacobian matrix are calculated numerically. At each iteration, the set of linear residual equations is inverted using a preconditioned conjugate gradient solver; see Reference [42] for details about the numerical implementation and user

features. All analyses discussed in the following subsections are performed within the iTOUGH2 simulation-optimization framework [44], which performs forward simulations; solves the inverse problem; and conducts sensitivity, uncertainty, and data-worth analyses.

2.4. Model Setup

We simulate the coupled fluid flow and heat transfer processes described in Section 2.2 within the two-dimensional, radial model domain shown in Figure 1. The model domain is discretized into cylindrical shell elements, each with an axial length of 0.5 inches (0.0127 m). The total length of the model domain in axial direction is adjustable between 12.0 inches (0.3048 m) and 84.0 inches (2.1336 m) to accommodate different separation distances between waste capsules. In radial direction, the first 100 shells have a constant thickness of 0.125 inches (0.003175 m) up to a radius of 12.5 inches (0.3175 m), after which the shell thicknesses increase logarithmically until the outer model domain radius of 3600 inches (91.44 m) is reached. The model has a total of 22,008 elements and 43,717 connections between them. Three equations (for the three primary variables pressure, saturation, and temperature) are solved at each point in space and time.

No-flow boundaries are specified at the symmetry planes. At the outer model domain radius, a Dirichlet boundary condition is specified with a pressure of 100 bar and a temperature of 40 °C, representative of a horizontal waste disposal section at a depth of 1 km. The same values are used as initial conditions throughout the model domain. As heat transfer is only mildly impacted by the absolute pressure and temperature values, we report our results as temperature changes with respect to the initial temperature of 40 °C.

A transient simulation for a duration of 30 years is performed with automatic time-step adjustment based on the convergence behavior of the Newton–Raphson iterations. The temperature change is extracted at the center of the waste capsule ($X = 0.0$; see Figure 1c) and for select radial distances, each representing a component of the engineered barrier system. Response surfaces are created for the maximum temperature change, which is extracted by fitting a polynomial through the three highest points of the discrete time series and setting its derivative to zero.

The key material properties are summarized in Table 1. These are reference material properties that will be adjusted over a considerable range to account for different selections of backfill materials and potential host rocks.

Table 1. Reference parameter set.

Material	Parameter	Units	Value	Range ¹
capsule	thermal conductivity, K	$\text{W m}^{-1} \text{K}^{-1}$	11.9	8.0–40.0
	solid density, ρ_s	kg m^{-3}	5500.0	n/a
	solid specific heat, c_s	$\text{J kg}^{-1} \text{K}^{-1}$	427.0	400.0–700.0
	permeability, k	m^2	0.0	n/a
canister	thermal conductivity, K	$\text{W m}^{-1} \text{K}^{-1}$	13.0	8.0–40.0
	solid density, ρ_s	kg m^{-3}	8000.0	n/a
	solid specific heat, c_s	$\text{J kg}^{-1} \text{K}^{-1}$	490.0	400.0–700.0
	permeability, k	m^2	0.0	n/a
casing	thermal conductivity, K	$\text{W m}^{-1} \text{K}^{-1}$	40.0	8.0–40.0
	solid density, ρ_s	kg m^{-3}	7670.0	n/a
	solid specific heat, c_s	$\text{J kg}^{-1} \text{K}^{-1}$	460.0	400.0–700.0
	permeability, k	m^2	0.0	n/a
backfill ²	thermal conductivity, K	$\text{W m}^{-1} \text{K}^{-1}$	2.0	0.5–3.0
	solid density, ρ_s	kg m^{-3}	2650.0	n/a
	solid specific heat, c_s	$\text{J kg}^{-1} \text{K}^{-1}$	880.0	700.0–900.0
	porosity, ϕ	%	40.0	n/a
	permeability, k	$\log(\text{m}^2)$	−16.0	n/a

Table 1. Cont.

Material	Parameter	Units	Value	Range ¹
host rock ³	thermal conductivity, K	$\text{W m}^{-1} \text{K}^{-1}$	2.0	0.5–3.0
	solid density, ρ_s	kg m^{-3}	2710.0	n/a
	solid specific heat, c_s	$\text{J kg}^{-1} \text{K}^{-1}$	850.0	700.0–900.0
	porosity, ϕ	%	5.0	n/a
	permeability, k	$\log(\text{m}^2)$	−17.0	n/a
waste	initial heat load, Q_{H0}	W/capsule	100.0	50.0–200.0
	capsule spacing, Δx	m	1.0	0.61–4.30

¹ Lower and upper bounds of parameters, defining the range examined by global sensitivity analysis and response surfaces; n/a: not applicable, i.e., parameter is fixed. ² Backfill of canister, casing, and annulus; each may consist of a different material, e.g., quartz sand, bentonite, drilling mud, or cement; properties to be selected based on chosen backfill material. ³ Various host rocks may be considered, including sedimentary, magmatic, and metamorphic rocks; properties to be selected based on site-specific host rock.

2.5. Local and Global Sensitivity Analyses

In addition to calculating the temperature evaluation for the reference parameter set of Table 1 and some discrete variants, we also perform extensive local and global sensitivity analyses and a data-worth analysis. Local sensitivity coefficients are needed to calculate composite sensitivity measures and to calculate estimation and prediction uncertainties. The local sensitivity coefficients are the partial derivatives of an output variable z_i with respect to an input parameter p_j , evaluated at the reference parameter set \mathbf{p}^* :

$$S_{ij} = \left. \frac{\partial z_i}{\partial p_j} \right|_{\mathbf{p}^*}. \quad (4)$$

To make S_{ij} dimensionless and comparable across different types of parameters and observations, they are scaled as follows:

$$\bar{S}_{ij} = S_{ij} \cdot \frac{\sigma_{p_j}}{\sigma_{z_i}}, \quad (5)$$

Here, where σ_p is the input- or parameter-scaling factor, and σ_z is the output- or observation-scaling factor. In the context of a sensitivity analysis, σ_p is the expected parameter variation, and σ_z denotes the threshold at which a change in the model prediction is considered significant. In the context of a data-worth analysis (see below), σ_p is interpreted as the acceptable parameter uncertainty, and σ_z is the expected mean residual obtained after the inversion, or the acceptable prediction uncertainty of the target predictions (for details, see References [44]).

A local sensitivity analysis indicates the relative influence of each of the unknown, uncertain, or variable parameters on the target predictions, which in our case are the maximum temperatures at specific points within the repository system. However, if the model is nonlinear, the sensitivity coefficients depend on the parameter set, which varies considerably during the early design stages of a project. We therefore employ a global sensitivity analysis method to identify the overall most influential parameters. Global sensitivity methods are comprehensively described in Reference [45]. As any global method, the Morris one-at-a-time (MOAT) elementary effects method [46] examines many parameter combinations within the range of acceptable values. In The MOAT method, the n -dimensional parameter hypercube is subdivided along each axis into $r - 1$ intervals, resulting in r^n grid points. For each parameter j , a perturbation Δ is calculated as:

$$\Delta_j = \frac{r}{2(r-1)} \cdot (p_{j,max} - p_{j,min}). \quad (6)$$

With a parameter set selected from a random grid point, the performance measure z is evaluated by the model. Each parameter p_j is perturbed in turn by Δ_j , z is recalculated, and the impact on the output (referred to as elementary effect, EE_j) is computed as:

$$EE_j = \frac{z(p_1, p_2, \dots, p_j + \Delta_j, \dots, p_n) - z(p_1, p_2, \dots, p_n)}{\Delta_j}. \quad (7)$$

EE_j is referred to as the elementary effect. EE_j is repeatedly evaluated, starting at randomly selected points. After several such paths within the parameter space have been explored, the mean and standard deviation of the absolute elementary effects (denoted by \overline{EE} and σ_{EE} , respectively) are determined. \overline{EE}_j reflects the composite influence of parameter j on the output, whereas $\sigma_{EE,j}$ identifies nonlinearities and interactions of the effect. We also create response surfaces for pairs of the most important design factors identified by the global sensitivity analysis.

2.6. Data-Worth Analysis

Finally, a data-worth analysis is done with the goal to design an experiment in which the key parameters affecting maximum temperatures can be determined with sufficient accuracy. A data-worth analysis identifies and ranks the relative contribution a data point makes when used in an inversion (e.g., for the estimation of thermal properties) and a subsequent predictive simulation (e.g., of maximum repository temperatures). The approach used in this study is described in Reference [47]. It is based on sensitivity coefficients, a linear estimation error analysis (to obtain the uncertainty in the estimated parameters given the available data and their uncertainties), and a linear uncertainty propagation analysis (to obtain the prediction uncertainty given uncertainty in the estimated parameters).

We denote n as the number of uncertain parameters that will be estimated based on m discrete measurements, i.e., n is the length of the parameter vector \mathbf{p} , and m is the length of the observation vector \mathbf{z} . Note that m changes during a data-worth analysis, as individual data points (or entire data sets) are either removed from the reference data set or added as potential observations. The covariance matrix of the estimated parameters, \mathbf{C}_{pp} , is calculated as:

$$\mathbf{C}_{pp} = (\mathbf{J}^T \mathbf{C}_{zz}^{-1} \mathbf{J})^{-1}. \quad (8)$$

Here, \mathbf{J} is the $m \times n$ Jacobian matrix, holding the sensitivity coefficients S_{ij} ; \mathbf{C}_{zz} is the $m \times m$ observation covariance matrix, containing the variances σ_z^2 on its diagonal.

A linear uncertainty propagation analysis is performed to yield the covariance matrix of the model predictions:

$$\mathbf{C}_{\hat{z}\hat{z}} = \hat{\mathbf{J}} \mathbf{C}_{pp} \hat{\mathbf{J}}^T. \quad (9)$$

Here, the Jacobian matrix $\hat{\mathbf{J}}$ contains the partial derivatives of the predictions with respect to the parameters. These sensitivity coefficients propagate the uncertainties in the parameters (described by \mathbf{C}_{pp}) to the predictions of interest.

In a data-worth analysis, the estimation and prediction uncertainty matrices, \mathbf{C}_{pp} and $\mathbf{C}_{\hat{z}\hat{z}}$, respectively, are re-evaluated for different calibration data sets. The data worth, $\omega_{\pm k}$, is then defined as the relative increase or decrease in the prediction uncertainty (measured by the trace of $\mathbf{C}_{\hat{z}\hat{z}}$) caused by the removal or addition of data. Starting with a set of reference data, the uncertainty analyses of Equations (8) and (9) determine whether the target values can be predicted with sufficiently low uncertainty, making it acceptable for the objectives of the modeling study. If it is acceptable, the data-worth analysis suggests which data could be removed, resulting in a less complex and less expensive design with minor impact on the accuracy of the estimated parameters and without markedly increasing prediction uncertainty. If uncertainties are unacceptably high, the

data-worth analysis indicates which supplementary data shall most effectively reduce the estimation and prediction uncertainty.

3. Results

3.1. Temperature Evolution

The temperature evolution at various radial distances from the center of the capsule (representing different components of the system) is shown in the left column of Figure 3 for three different capsule spacings; the time-dependent decay-heat power output for one capsule is also shown. The simulated temperature distribution 3 years after the emplacement of heat-generating waste capsules is shown in the right column. As expected, temperatures are higher if waste capsules are emplaced end-to-end with very little separation distance, and maximum temperature changes are reduced if the capsules are spaced farther apart. However, the relative reduction in maximum temperature becomes smaller for larger separation distances, as the heat dissipation regime transitions from cylindrical (Figure 3a) to approximately spherical (Figure 3c). As a result, only small benefits regarding maximum temperature can be gained by spacing capsules by more than about 2 m.

For an initial heat output of 100 W per capsule, a dense capsule emplacement configuration with a spacing of 2 ft (0.6096 m) leads to maximum temperature increases of about 73 °C for the capsule itself, and about 60 °C at the drillhole wall. Recall that these temperature increases are proportional to the heat output. To avoid boiling in the backfill material between the canister and the casing, the initial heat output must be limited to about 360 W in a drillhole that is at a depth of 1 km at an ambient temperature of 40 °C, as inferred from the boiling curve of Figure 2 and the maximum temperature increase shown in Figure 1a. Note that none of the cesium capsules and only a small fraction of the strontium capsules generate heat in excess of 360 W [34,35]. These capsules can be stored at the surface for a longer period, or placed in the horizontal drillhole with an appropriately increased separation distance to their neighbors. In general, a slightly broadened emplacement pattern should be used to account for uncertainties in heat output, in ambient temperature and pressure, and in the thermal properties of the various materials, in particular the host rock, whose heat conductivity is most uncertain, most variable, and at the same time most influential, as demonstrated in the following sensitivity analyses.

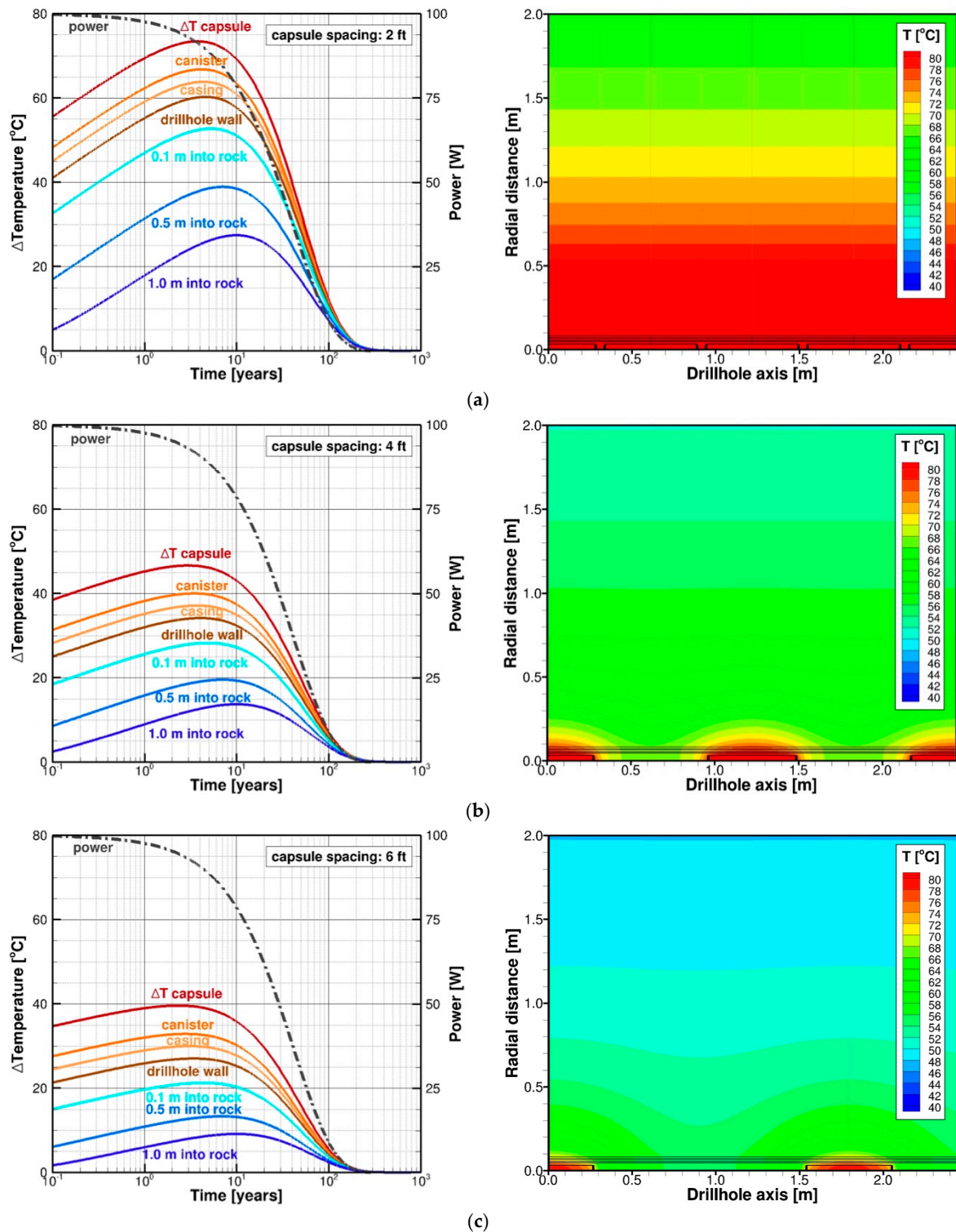


Figure 3. Evolution of temperature change and decay-heat output (left column) and temperature distribution after 3 years (right column) for an initial heat release of 100 W per waste capsule with capsule spacings of (a) 2 ft (0.6096 m); (b) 4 ft (1.219 m); and (c) 6 ft (1.829 m).

3.2. Sensitivity Analyses

We performed local and global sensitivity analyses to obtain insights into the system behavior and to identify influential and non-influential parameters. We also mapped out maximum temperature

changes over a wide range of the most influential parameters, creating response surfaces as a convenient design tool.

For the drillhole disposal concept, heat dissipation is almost exclusively in the radial direction, passing through different materials that are arranged in concentric, cylindrical shells. Because of this configuration, the components are encountered in series, and, consequently, heat flow is controlled by the components of relatively low thermal diffusivity. The metallic elements with a high thermal conductivity and small shell thickness (i.e., the canister and casing) are expected to have an insignificant impact on the spatial and temporal temperature distribution. This is confirmed by a local sensitivity analysis, which is performed for a capsule spacing of 48 inches (1.22 m). A composite sensitivity measure—defined as the sum of the absolute values of the scaled sensitivity coefficients (Equation (5)) for each column and row of the sensitivity matrix—is calculated for each thermal parameter (columns of \bar{S}) and the maximum temperature at select locations (rows of \bar{S}). We also evaluated the impact of a 10% change in the heat output on the maximum temperature.

Table 2 indicates that the heat conductivity of the host rock is the most influential parameter, followed by the strength of the heat source. As expected, a 10% change in rock thermal conductivity has about the same impact as a 10% change in heat output. The conductivity of the canister backfill material has some effect on the capsule temperature, but not on the temperatures outside the canister. The thermal properties of the capsule, canister and casing are essentially irrelevant if fabricated with highly conductive material. As heat dissipates in a radially outward direction, the composite sensitivity measures for the observations generally decline with radial distance from the drillhole axis. The thermal conductivity of the host rock has its maximum influence at the drillhole wall, where the observation is collocated with the domain the parameter refers to. These general insights are quite robust with respect to the somewhat subjective choice of the parameter scaling factor, i.e., even if the uncertainties in thermal conductivity vary between materials, this does not substantially affect the qualitative statements made above.

Table 2. Scaled sensitivity coefficients \bar{S}_{ij} and composite sensitivity measures.

Data ²	Parameters ¹								
	$K_{capsule}$	K_{back1}	$K_{canister}$	K_{back2}	K_{casing}	$K_{annulus}$	K_{rock}	Q_{heat}	$\Sigma \bar{S}_j$
$T_{capsule}$	0.13	2.76	0.06	1.25	0.05	1.18	14.25	4.67	24.35
$T_{canister}$	0.02	0.06	0.06	1.25	0.05	1.18	14.36	4.00	20.98
T_{casing}	0.02	0.05	0.03	0.02	0.05	1.18	14.44	3.72	19.51
$T_{rock\ 0.0\ m}$	0.01	0.04	0.02	0.02	0.04	0.12	14.61	3.42	18.28
$T_{rock\ 0.1\ m}$	0.01	0.02	0.01	0.01	0.02	0.06	12.22	2.83	15.18
$T_{rock\ 0.5\ m}$	0.00	0.01	0.01	0.00	0.00	0.00	8.28	1.96	10.26
$T_{rock\ 1.0\ m}$	0.00	0.00	0.00	0.00	0.00	0.00	5.51	1.37	6.88
$\Sigma \bar{S}_i$	0.19	2.94	0.19	2.55	0.21	3.72	83.67	21.97	-

¹ The parameter scaling factor for thermal conductivities and heat output are $\sigma_K = 1.0$ and $\sigma_Q = 10.0$, respectively; subscripts back1 and back2 refer to the backfill material between the capsule and the canister, and between the canister and the casing, respectively; the sensitivity coefficient for heat capacity and material densities are significantly smaller and are thus not tabulated. ² Observations of interest are the maximum temperatures encountered during the repository lifetime; $T_{rock\ X\ m}$ is the maximum temperature in the rock X m from the drillhole wall; as only temperatures are considered, the observation scaling factor is irrelevant—it is set to $\sigma_T = 1.0$.

The local sensitivity analysis is contingent on the chosen reference parameter set (see Table 1). Therefore, a Morris global sensitivity analysis is able to test the validity of the simple local sensitivity analysis and to examine nonlinearity and interaction effects. The parameters involved in this global sensitivity analysis and their upper and lower bounds (defining the parameter hypercube) are listed in Table 1 above. The 12-dimensional parameter hypercube is subdivided into $r - 1 = 5$ intervals and examined along $n_p = 40$ paths, as described in Section 2.6.

Figure 4 shows a cross-plot between the mean and standard deviation of the absolute elementary effect (EE ; Equation (7)) of the Morris global sensitivity analysis. The dashed line represents

$|\overline{EE}| = 2 \cdot \sigma_{\overline{EE}}$, where $\sigma_{\overline{EE}} = \sigma_{EE} / \sqrt{n_p}$ is the standard error of the mean of the elementary effect. All the parameters are below the dashed line, indicating that their non-zero impacts are statistically significant. By far the most influential parameters are the heat output (red circle), the host rock's thermal conductivity (blue diamond), and the capsule spacing (black X). With the exception of the host rock's heat capacity (blue triangle), thermal conductivities (diamonds) are considerably more influential than the heat capacities (triangles) for all other components. Properties that are closer to the drillhole axis (hot colors) are less influential than those further out (cool colors), with the exception of the capsule's heat capacity (red triangle), which influences the maximum temperature of the waste capsule. The parameters also have considerable non-zero standard deviations, indicating that they exhibit interaction effects. This is expected as the temperature is essentially determined by a weighted harmonic average of all thermal diffusivities.

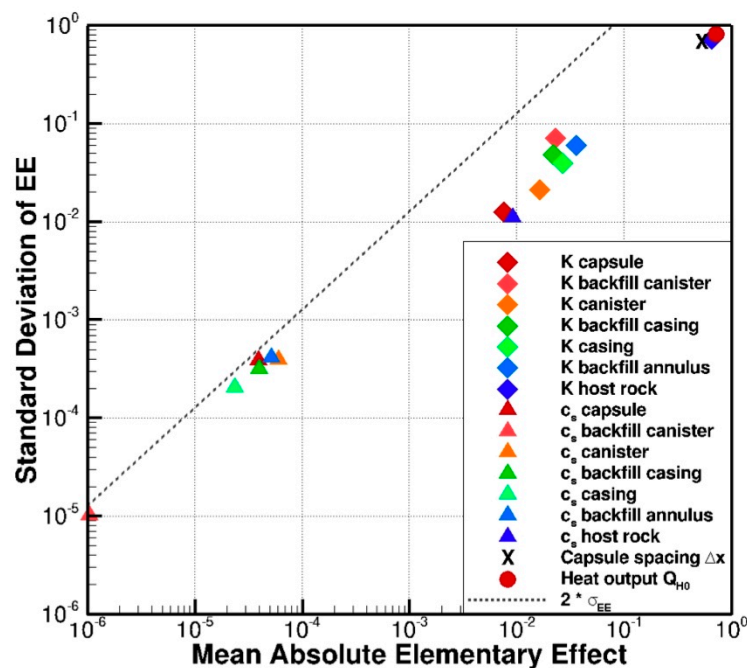


Figure 4. Mean absolute elementary effect and standard deviation for each parameter examined using the Morris global sensitivity analysis.

The global sensitivity analysis corroborates the parameter ranking previously obtained by the local, composite sensitivity measures. While the capsule spacing is an adjustable design parameter and the heat output of the waste capsule is well known, the host rock's heat conductivity is the main parameter that needs to be accurately determined. Any unacceptably high estimation uncertainty in this influential parameter will be propagated to high uncertainties in the predicted maximum repository temperatures. This will be addressed by the data-worth analysis, which helps reduce the estimation uncertainties of the parameters that are most influential on the model prediction of interest.

3.3. Response Surfaces

Figure 5 shows two-dimensional response surfaces of the maximum temperature increase at select radial locations as a function of thermal conductivity of the host rock and capsule spacing. Host-rock conductivity is chosen because it is the most influential property that may also vary over a considerable range depending on the rock type and spatial heterogeneity. Capsule spacing is selected as the main design parameter that can be adjusted for effective temperature control.

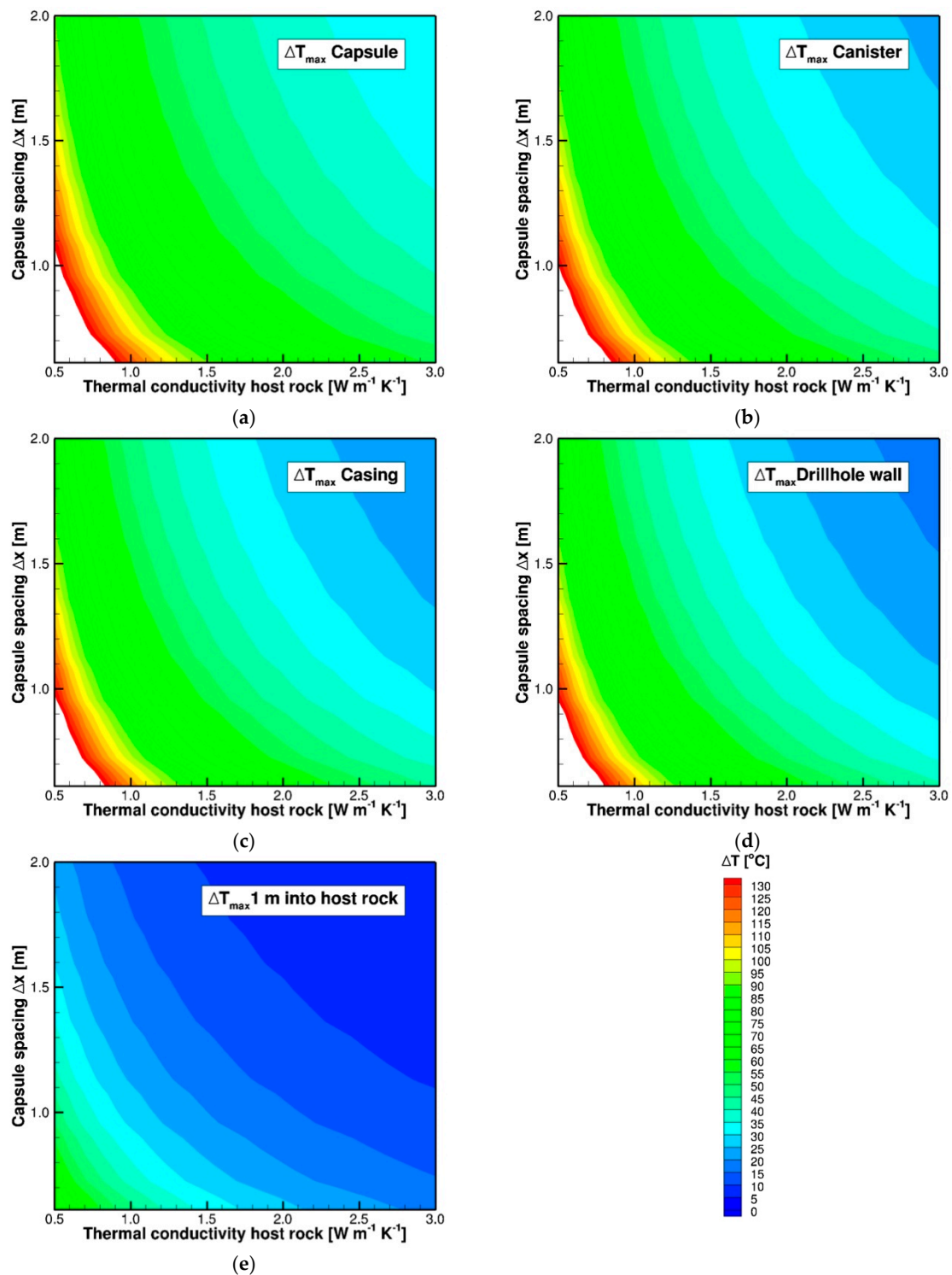


Figure 5. Response surfaces of maximum temperature increase as a function of host-rock thermal conductivity and capsule spacing for a 100 W initial heat output for the following repository components: (a) waste capsule; (b) canister; (c) casing; (d) drillhole wall; and (e) host rock 1 m from the drillhole wall.

To obtain the actual temperature for a given combination of host-rock thermal conductivity and capsule spacing, the value from the response surface must be multiplied by the heat output factor $f_H = Q_{H0}/100 \text{ W}$, and the result added to the ambient temperature at the depths of the disposal zone. Parameter combinations in the white corners of the response surfaces would lead to boiling if

waste capsules with a heat output of 200 W were disposed in a horizontal drillhole at a depth of 1 km. (Recall that thermal criteria other than the boiling temperature may be relevant.) These response surfaces can be directly used to determine an appropriate capsule spacing given the relevant maximum temperature criterion for each of the repository components and the in situ thermal conductivity of the host rock.

Figure 6 shows the impact of backfill thermal conductivities on the maximum capsule and drillhole wall temperatures. The backfill between the canister and the casing may be a drilling mud, a slurry, sand, bentonite, cement, or another suitable material; the annulus backfill (between the casing and the drillhole wall) is most likely either drilling mud or cement. The lower bound of the thermal conductivity range examined in these response surfaces represents a slurry or accounts for the presence of a fluid-filled gap. Only if backfill conductivities approach these lower bounds does temperature increase slightly relative to the reference case. Note that the temperature ranges in the two response surfaces of Figure 6 are much smaller compared to those shown in Figure 5, confirming the lower influence of these two parameters. For thermal conductivities above about $1.5 \text{ W m}^{-1} \text{ K}^{-1}$, the sensitivity of the capsule temperature becomes small and essentially disappears for the drillhole wall temperature. Note that increasing thermal conductivities of the backfill materials leads to faster heat dissipation away from the capsule, thus cooling it down, while speeding up the outward propagation of the heat pulse, thus leading to increased maximum temperatures at the drillhole wall.

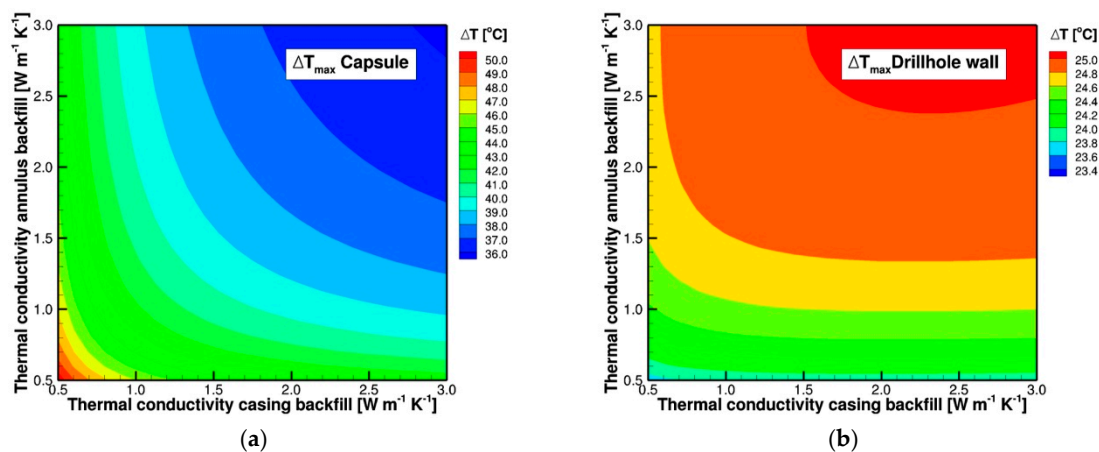


Figure 6. Response surfaces of maximum temperature increase as a function of casing-backfill and annulus thermal conductivities for a 100 W initial heat output for the following repository components: (a) waste capsule; and (b) drillhole wall.

3.4. Data-Worth Analysis

The purpose of the data-worth analysis is to design an in situ heater test that determines influential thermal properties with sufficient accuracy so that the maximum temperature throughout the drillhole and adjacent host rock can be predicted with acceptable uncertainty. The basic idea is to insert a capsule containing an electrical heater into the disposal section of the drillhole, backfill the test section according to the design specifications, then start releasing heat at a controlled wattage. Next, the temperature evolution data are recorded by a distributed temperature sensor (DTS). A DTS system uses a laser backscattering technique to measure temperatures continuously along an optical sensor cable, resulting in data with high spatial and temporal resolution [48]. The temperature data are inverted to determine key properties, specifically the host rock thermal conductivity. Once the thermal properties are identified, the response surfaces of Figure 5 can be used to determine the appropriate spacing of the actual waste capsules.

The data-worth analysis provides quantitative measures that help determine the number and location of the temperature sensors and the duration of the heating experiment. Two models—referred to as the calibration and prediction models—need to be developed and run sequentially. The

calibration model simulates the heater test data, whereas the prediction model simulates the maximum temperatures induced by the disposal of heat-generating nuclear waste. The calibration model covers the short duration of the heater test; the prediction model covers the much longer duration of the thermal period.

For the reference test, we consider a single heater the size of an actual waste capsule, heating at a constant output of 200 W for up to 30 days. We measure temperature at a DTS sensor attached to the casing. We expect that these temperature data can be matched by the calibration model with an average residual of 1 °C. This standard deviation is chosen to be larger than the measurement accuracy of DTS of about 0.1 °C to account for model simplifications. Should the quantity and quality of these measurements not allow for an accurate estimation of the key thermal properties, we consider installing additional DTS sensors at the surface of the heater and the drillhole wall to collect supplementary temperature data. Moreover, we introduce some prior information about the thermal conductivities and heat capacities, reflecting independent property measurements on engineered materials (metals and backfill) as well as retrieved drill core samples or cutting fragments of the host rock. However, we do not rely on this information to be very accurate; we mainly use it to stabilize the solution of the notional inverse problem (Equation (8)). Uncertainty in the heater output is also considered by estimating it during the inversion, with a standard deviation of 20 W assigned to its prior information value.

Figure 7 shows the temperature increase and data-worth metric as a function of heating time. The temperature increase exceeds 20 °C after less than 2 days, and reaches 40 °C after 30 days of heating, with only slightly higher temperatures at the heater compared to the drillhole wall. The dimensionless data-worth metric measures the relative reduction in uncertainty of the predicted maximum repository temperatures as data are added. Data worth increases sharply during the initial days of heating. At later times, the data worth, which accounts for parameter correlations and redundancies of closely spaced data points, approaches a constant value. This indicates that the information content of the DTS data initially grows quickly, but is reduced to a constant rate as the heater test is prolonged. Accurately measuring temperatures at early times is most beneficial, with later data providing additional, albeit less important information. The test can be terminated once the acceptable prediction uncertainty is achieved.

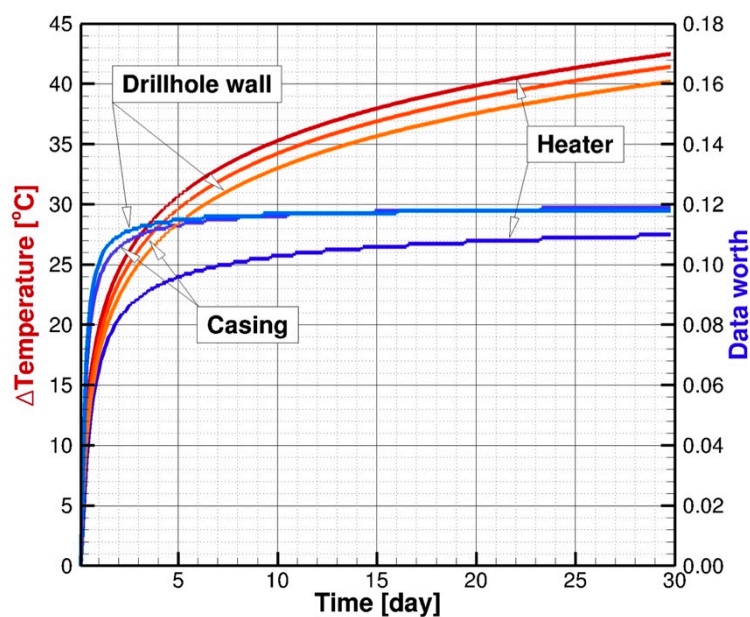


Figure 7. Temperature increase and data-worth metric for distributed temperature sensors installed at different locations within the drillhole as a function of time.

Next we observe that no significant benefits can be gained by moving the DTS from the casing to the drillhole wall or towards the heater. Installation of the DTS fiber-optic cable by clamping it to the outside of the casing is not only most practical, but also desirable as it avoids interference of the cable with waste emplacement operations. We therefore decide to focus only on the DTS data collected along the casing, discarding the use of additional sensors.

We first discuss the results of the notional inversion, which is simply the evaluation of Equation (8) with the assumption that the match to the (still non-existent) data is consistent with the prior observation covariance matrix, C_{zz} . The resulting covariance matrix of the estimated parameters, C_{pp} , reveals that performing the heater test mainly helps determine the thermal conductivity of the host rock, as expected.

Table 3 shows the estimation and prediction uncertainties for different testing durations. Without conducting an in situ heater test, the uncertainty of the predicted maximum temperature is high. For example, on the 95% confidence level, the prediction of the maximum temperature change at the drillhole wall would read $\Delta T_{wall} = 34 \pm 30$ °C. Even granted that the normality and linearity assumptions underlying the uncertainty analysis of Equation (9) are violated, this large uncertainty renders the prediction essentially not very useful.

Table 3. Estimation and prediction uncertainties for select heater test durations.

Time (d)	Estimation		Prediction ¹					
	$\sigma_{K_{rock}}$	$\sigma_{T,capsule}$	$\sigma_{T,canister}$	$\sigma_{T,casing}$	$\sigma_{T,wall}$	$\sigma_{T,0.1m}$	$\sigma_{T,0.5m}$	$\sigma_{T,1.0m}$
0	1.00	14.8	14.6	14.6	14.7	12.3	8.3	5.6
1	0.28	2.9	2.1	2.1	2.8	2.3	1.6	1.0
2	0.25	2.7	1.5	1.3	2.0	1.7	1.1	0.8
5	0.20	2.7	1.2	0.8	1.2	1.0	0.7	0.5
10	0.16	2.7	1.1	0.7	0.9	0.7	0.5	0.3
20	0.14	2.7	1.1	0.6	0.6	0.5	0.3	0.2
30	0.13	2.7	1.1	0.6	0.5	0.4	0.2	0.2

¹ Uncertainty of predicted maximum component temperature during repository life time.

Performing a 1-day-long heater test, the estimation uncertainty of the most influential parameter, the host rock thermal conductivity, is reduced from its prior value of 1.0 to less than 0.3 W m⁻¹ K⁻¹. An even lower uncertainty can be achieved if the heater output is controlled accurately, a result of the fact that these two parameters are strongly correlated. Combined with uncertainty reductions in the other parameters that are concurrently estimated with K_{rock} leads to considerably improved temperature predictions. Specifically, the maximum temperature at the drillhole wall now reads $\Delta T_{wall} = 34 \pm 6$ °C. Whether such a prediction uncertainty is acceptable depends on its use for repository design and performance assessment. The uncertainties can be further reduced by prolonging the heater test, albeit with diminishing added value for the later times. If testing lasts for 10 days or longer, the uncertainty of the model-predicted maximum temperature experienced by the host rock at the drillhole wall is less than 1 °C.

4. Discussion

The temperature evolution in the disposal section of a horizontal drillhole was simulated for a wide range of thermal properties of engineered and natural materials. We specifically examined the maximum temperatures encountered during the thermal pulse period at selected locations within the drillhole and the near-field host rock. The sensitivity analyses indicate that the key factors affecting maximum temperatures are the thermal conductivity of the host rock, the spacing between waste capsules, and the wattage of the heat-generating waste. The global sensitivity analysis demonstrates that the identification of the most influential parameters is robust even if the reference property values are uncertain or variable over a wide range. Of these three influential parameters, only the heat conductivity of the host rock cannot be adjusted and needs to be determined for in situ conditions at

the selected disposal site. Should its value turn out to be too low (leading to excessive temperatures in the repository), a different layer needs to be chosen, or an altogether different site must be explored. The heat output of the waste can be partly controlled by extending the post-reactor cooling period in a surface storage facility. Finally, the spacing of waste within the drillhole is the main, readily adjustable design parameter used for thermal management of the repository.

The thermal properties of the backfill material have a much smaller impact on the maximum temperatures. Temperatures increase somewhat if backfill conductivities approach very small values. Such small values may only occur if a relatively wide, fluid-filled gap develops over the entire circumference of the canister, casing, or drillhole wall, acting as a relative insulator. Despite this possibility, it can be recommended that a suitable backfill material should be selected mainly based on its ability to fulfill a specific barrier function rather than because of its thermal properties.

We also examined the possibility of performing an in situ heater test to determine the thermal properties of the as-built repository system. From an operational point of view, the proposed heater test is well integrated into the site development and characterization process. After completion of the drillhole, the heater (which has the same dimensions as the waste canister) is pushed to the end of the disposal section, testing the integrity of the drillhole and the absence of obstructions, confirming that emplacement of actual waste capsules is possible. The short testing section is then instrumented and backfilled according to the design specifications, testing the corresponding procedures. Heating and data collection begins. While the heater experiment is running, the entire drillhole is available for logging, characterization and disposal preparation. Temperature data are analyzed in real time by performing inversions using a calibration model that will be set up in advance. Once sufficient data are collected such that the site-specific thermal properties are determined with the desired level of accuracy, the heater test can be terminated, and waste emplacement may commence. If there are indications of considerable heterogeneities along the drillhole, the heater test may be repeated at selected locations. Finally, the DTS sensors can be used to observe the thermal evolution along the disposal section as part of performance confirmation monitoring. The design of the heater experiment (including the way power is supplied) should be further optimized and tested in a pilot drillhole. If the main goal is only to determine the host rock's thermal conductivity under in situ conditions (i.e., without testing the thermal performance of the as-built engineered barrier system), a less intrusive approach using a combination of DTS and a borehole-length electrical resistance heater (a system referred to as distributed thermal perturbation sensor; see Reference [49]) could be considered.

5. Conclusions

The maximum temperature expected within a horizontal drillhole and the surrounding host formation is an important factor that mainly affects our ability to robustly predict repository performance. These temperatures need to be simulated with acceptably low prediction uncertainty in order to provide a defensible basis for the demonstration that they are below regulatory thermal limits. While such thermal limits are not discussed or proposed in this study, we recommend that repository temperatures remain below the boiling temperature under in situ conditions at all times to avoid the significant complexities arising from phase changes and the related coupled processes.

In general, the linear arrangement of waste capsules or spent nuclear fuel assemblies in a long horizontal drillhole leads to relatively large specific surface areas available for heat dissipation. Thermal management for a drillhole repository is thus less challenging compared to that for other repository concepts, where relatively large volumes of heat-generating waste are densely packed in mined caverns or large-diameter deposition holes. For a moderate capsule spacing of about 2 m, thermal interference is very small; denser loading of the disposal section of the drillhole can be justified using the design approach outlined in this paper. The simulations show that waste spacing is a very effective design parameter to manage temperatures in the disposal section of the drillhole.

The design calculations presented here were done for the disposal of relatively small, but thermally hot cesium and strontium capsules. The maximum temperatures for a cesium capsule, which typically

generates about 100 W at the time it is emplaced in the drillhole, are less than 100 °C above the ambient temperature, i.e., far below the in situ boiling temperature. Only a small fraction of the strontium capsules have high enough heat output to significantly raise the temperatures, but these cases can be readily managed by increasing the capsule spacing. The thermal maximum is reached after less than 10 years, i.e., a time much shorter than that predicted for a large, mined repository. Note that deep nuclear waste isolation in horizontal drillholes is considered feasible also for other waste forms, specifically SNF assemblies. The thermal analyses discussed in this paper need to be adapted for the specific geometry and heat output of these other waste forms.

While predominantly conductive heat transfer is appropriately captured by focusing on the local behavior in a short section of the repository, other processes (e.g., corrosion gas migration, regional fluid flow, radionuclide transport) may require that the entire drillhole (including the vertical access section) be modeled. Nevertheless, an overall approach similar to the one presented here can be used to examine such processes in support of repository design, uncertainty quantification, and performance assessment.

Parameters that are both influential and uncertain need to be carefully assessed prior to performing design calculations and uncertainty analyses. We have demonstrated through a data-worth analysis that a short-term in situ heater test is a viable approach to robustly identify the key factors affecting the temperature evolution in the repository. The main conceptual idea is to run a test that (a) uses the as-built configuration under in situ conditions (thus testing the actual disposal system), (b) examines the system at the actual scale (thus avoiding the need for upscaling), (c) perturbs the system using thermal stresses (thus invoking the relevant process), and (d) collects (temperature) data that are identical to the prediction variable of interest (thus avoiding the need for indirect inferences). A well-designed heater test, which can readily be integrated into the operation of a horizontal drillhole waste repository, is an effective, defensible way to obtain confidence in our understanding of the thermal system behavior, and to improve our ability to make robust predictions.

6. Patents

Finsterle S.; Muller, R.A.; Rector, J.W. Thermal evolution near heat-generating waste canisters in horizontal drillholes. U.S. Patent Application Serial No. 62/781,337, 18 December 2018.

Author Contributions: Conceptualization, S.F., R.A.M. and R.B.; Data curation, S.F., R.A.M. and J.P.; Formal analysis, S.F. and R.A.M.; Funding acquisition, R.A.M.; Investigation, S.F. and J.P.; Methodology, S.F., R.A.M. and R.B.; Project administration, R.A.M. and R.B.; Resources, R.A.M.; Software, S.F.; Supervision, R.A.M.; Validation, S.F., R.A.M. and J.W.R.; Visualization, S.F.; Writing—original draft, S.F.; Writing—review & editing, R.A.M., R.B., J.P. and J.W.R.

Acknowledgments: We thank three anonymous reviewers for their constructive comments. We also acknowledge Robert J. Budnitz and Per F. Peterson for their comments on an earlier draft of the manuscript.

Conflicts of Interest: The authors declare no conflict of interest.

References

1. Deep Isolation Technology. Available online: <https://www.deepisolation.com/technology/> (accessed on 25 January 2019).
2. Shoesmith, D.W. Assessing the corrosion performance of high-level nuclear waste containers. *Corrosion* **2006**, *62*, 703–722. [[CrossRef](#)]
3. Johnson, L.; King, F. The effect of the evolution of environmental conditions on the corrosion evolutionary path in a repository for spent fuel and high-level waste in Opalinus clay. *J. Nucl. Mater.* **2008**, *379*, 9–15. [[CrossRef](#)]

4. Hornus, E.C.; Giordano, C.M.; Rodríguez, M.A.; Carranza, R.M. Effect of Temperature on the Crevice Corrosion Resistance of Ni-Cr-Mo Alloys as Engineered Barriers in Nuclear Waste Repositories. Available online: <https://www.cambridge.org/core/journals/mrs-online-proceedings-library-archive/article/effect-of-temperature-on-the-crevice-corrosion-resistance-of-nicrmo-alloys-as-engineered-barriers-in-nuclear-waste-repositories/3004CB4697C551D8F95AF0D4BFAABAC4> (accessed on 12 February 2019).
5. Werme, L.; Björner, I.K.; Bart, G.; Zwicky, H.U.; Grambow, B.; Lutze, W.; Ewing, R.C.; Magrabi, C. Chemical corrosion of highly radioactive borosilicate nuclear waste glass under simulated repository conditions. *J. Mater. Res.* **1990**, *5*, 1130–1146. [[CrossRef](#)]
6. Shoesmith, D.W. Fuel corrosion processes under waste disposal conditions. *J. Nucl. Mater.* **2000**, *282*, 1–31. [[CrossRef](#)]
7. Pusch, R.; Madsen, F.T. Aspects on the illitization of the kinnekulle bentonites. *Clays Clay Miner.* **1995**, *43*, 261–270. [[CrossRef](#)]
8. Kamei, G.; Mitsui, M.S.; Futakuchi, K.; Hashimoto, S.; Sakuramoto, Y. Kinetics of long-term illitization of montmorillonite—A natural analogue of thermal alteration of bentonite in the radioactive waste disposal system. *J. Phys. Chem. Solids* **2005**, *66*, 612–614. [[CrossRef](#)]
9. Turick, C.E.; Berry, C.J. Review of concrete biodeterioration in relation to nuclear waste. *J. Environ. Radioact.* **2016**, *151*, 12–21. [[CrossRef](#)]
10. Tassoni, E.; Gera, F. Disposal of high-level radioactive waste in argillaceous formations: In-Situ and laboratory heating experiments. *Nucl. Technol.* **1986**, *72*, 89–98. [[CrossRef](#)]
11. Horseman, S.T.; McEwen, T.J. Thermal constraints on disposal of heat-emitting waste in argillaceous rocks. *Eng. Geol.* **1996**, *41*, 5–16. [[CrossRef](#)]
12. Bossart, P.; Jaeggi, D.; Nussbaum, C. Experiments on thermo-hydro-mechanical behaviour of Opalinus Clay at Mont Terri rock laboratory, Switzerland. *Rock Mech. Geotech. Eng.* **2017**, *9*, 502–510. [[CrossRef](#)]
13. Nguyen, T.S.; Selvadurai, A.P.S.; Armand, G. Modelling the FEBEX THM experiment using a state surface approach. *Int. J. Rock Mech. Min. Sci.* **2005**, *42*, 639–651. [[CrossRef](#)]
14. Zheng, L.; Samper, J.; Montenegro, L.; Fernández, A.M. A coupled THMC model of a heating and hydration laboratory experiment in unsaturated compacted FEBEX bentonite. *J. Hydrol.* **2011**, *386*, 80–94. [[CrossRef](#)]
15. Kumpalainen, S.; Kiviranta, L.; Korkeakoski, P. Long-term effects of an iron heater and Äspö groundwater on smectite clays: Chemical and hydromechanical results from the in situ alternative buffer material (ABM) test package 2. *Clay Miner.* **2016**, *51*, 129–144. [[CrossRef](#)]
16. Gens, A.; Garcia-Molina, A.J.; Olivella, S.; Alonso, A.A.; Huertas, F. Analysis of a full scale in situ test simulating repository conditions. *Int. J. Numer. Anal. Meth. Geomech.* **1998**, *22*, 515–548. [[CrossRef](#)]
17. Gens, A.; Sánchez, M.; Guimarães, L.; Alonso, A.A.; Loret, A.; Olivella, S.; Villar, M.V.; Huertas, F. A full-scale in situ heating test for high-level nuclear waste disposal: Observations, analysis and interpretation. *Géotechnique* **2009**, *59*, 377–399. [[CrossRef](#)]
18. Rutqvist, J.; Barr, D.; Birkholzer, J.T.; Chijimatsu, M.; Kolditz, O.; Liu, Q.; Oda, Y.; Wang, W.; Zhang, C. Results from an international simulation study on coupled thermal, hydrological, and mechanical processes near geological nuclear waste repositories. *Nucl. Technol.* **2008**, *163*, 101–109. [[CrossRef](#)]
19. Chen, Y.; Zhou, C.; Jing, L. Modeling coupled THM processes of geological porous media with multiphase flow: Theory and validation against laboratory and field scale experiments. *Comput. Geotech.* **2009**, *36*, 1308–1329. [[CrossRef](#)]
20. Sánchez, M.; Gens, A.; Olivella, S. THM analysis of a large-scale heating test incorporating material fabric changes. *Int. J. Numer. Anal. Meth. Geomech.* **2012**, *36*, 391–421. [[CrossRef](#)]
21. Tsang, Y.W.; Birkholzer, J.T. Predictions and observations of the thermal-hydrological conditions in the Single Heater Test. *J. Contam. Hydrol.* **1999**, *38*, 385–425. [[CrossRef](#)]
22. Birkholzer, J.T.; Tsang, Y.W. Modeling the thermal-hydrologic processes in a large-scale underground heater test in partially saturated fractured tuff. *Water Resour. Res.* **2000**, *36*, 1431–1447. [[CrossRef](#)]
23. Buscheck, T.A.; Rosenberg, N.D.; Gansemer, J.; Sun, Y. Thermohydrologic behavior at an underground nuclear waste repository. *Water Resour. Res.* **2002**, *38*. [[CrossRef](#)]
24. Buscheck, T.A.; Glascoe, L.G.; Lee, K.H.; Gansemer, J.; Sun, Y.; Mansoor, K. Validation of the Multiscale Thermohydrologic Model used for analysis of a proposed repository at Yucca Mountain. *J. Contam. Hydrol.* **2004**, *62*, 421–440. [[CrossRef](#)]

25. Haukwa, C.B.; Wu, Y.-S.; Bodvarsson, G.S. Modeling thermal-hydrological response of the unsaturated zone at Yucca Mountain, Nevada, to thermal load at a potential repository. *J. Contam. Hydrol.* **2004**, *62–63*, 529–552. [[CrossRef](#)]
26. Webb, S.W.; Francis, N.D.; Dunn, S.D.; Itamura, M.T.; James, D.L. Thermally induced natural convection effects in Yucca Mountain Drifts. *J. Contam. Hydrol.* **2004**, *62*, 713–730. [[CrossRef](#)]
27. Rutqvist, J.; Barr, D.; Datta, R.; Gens, A.; Millard, A.; Olivella, S.; Tsang, C.-F.; Tsang, Y. Coupled thermal–hydrological–mechanical analyses of the Yucca Mountain Drift Scale Test—Comparison of field measurements to predictions of four different numerical models. *Int. J. Rock Mech. Min. Sci.* **2005**, *42*, 680–697. [[CrossRef](#)]
28. Brady, P.V.; Arnold, B.W.; Freeze, G.A.; Swift, P.N.; Bauer, S.J.; Kanney, J.L.; Rechar, R.P.; Stein, J.S. *Deep Borehole Disposal of High-Level Radioactive Waste*; Report SAND2009-4401; Sandia National Laboratories: Albuquerque, NM, USA, 2009; p. 75.
29. Hansen, F.D.; Hardin, E.L.; Rechar, R.P.; Freeze, G.A.; Sassani, D.C.; Brady, P.V.; Stone, C.M.; Martinez, M.J.; Holland, J.F.; Dewers, T.; et al. *Shale Disposal of U.S. High-Level Radioactive Waste*; Report SAND2010-2843; Sandia National Laboratories: Albuquerque, NM, USA, 2010; p. 148.
30. Hardin, E.L. *Deep Borehole Field Test Conceptual Design Report*; Report SAND2016-10246R; Sandia National Laboratories: Albuquerque, NM, USA, 2016; p. 312.
31. Gibb, F.G.F.; Travis, K.P.; McTaggart, N.A.; Burley, D. A model for heat flow in deep borehole disposals of high-level nuclear waste. *J. Geophys. Res.* **2008**, *113*, B05201. [[CrossRef](#)]
32. Gibb, F.G.F.; Travis, K.P.; McTaggart, N.A.; Burley, D.; Hesketh, K.W. Modeling temperature distribution around deep borehole disposals of HLW. *Nucl. Technol.* **2008**, *163*, 62–73. [[CrossRef](#)]
33. Forsberg, C.W. Rethinking high-level waste disposal: Separate disposal of high-heat radionuclides (^{90}Sr and ^{137}Cs). *Nucl. Technol.* **2000**, *131*, 252–268. [[CrossRef](#)]
34. SNL (Sandia National Laboratories). *Evaluation of Options for Permanent Geologic Disposal of Spent Nuclear Fuel and High-Level Radioactive Waste in Support of a Comprehensive National Nuclear Fuel Cycle Strategy, Volumes I and II (Appendices)*; SAND2014-0187P (Vol. 1), SAND2014-0189P (Vol. II); Sandia National Laboratories: Albuquerque, NM, USA, 2014.
35. Price, L. Overview of Cesium and Strontium Capsules for Deep Borehole Disposal. In Proceedings of the International Meeting on Deep Borehole Disposal of High-Level Radioactive Waste, Sheffield, UK, 13–15 June 2016; Sandia National Laboratories: Albuquerque, NM, USA, 2016.
36. Stauffer, P.H.; Lewis, K.C.; Stein, J.S.; Travis, B.J.; Lichtner, P.; Zvoloski, G. Joule-Thomson effect on the flow of liquid water. *Transp. Porous Med.* **2014**, *104*, 471–485. [[CrossRef](#)]
37. Zheng, L.; Rutqvist, J.; Birkholzer, J.T.; Liu, H.-H. On the impact of temperatures up to 200 °C in clay repositories with bentonite engineer barrier systems: A study with coupled thermal, hydrological, chemical, and mechanical modeling. *Eng. Geol.* **2015**, *197*, 278–295. [[CrossRef](#)]
38. Jury, W.A.; Horton, R. *Soil Physics*, 6th ed.; John Wiley & Sons, Inc.: Hoboken, NJ, USA, 2004; pp. 181–184. ISBN 0-471-05965-X.
39. Askari, R.; Taheri, S.; Hejazi, S.H. Thermal conductivity of granular porous media: A pore scale modeling approach. *AIP Adv.* **2015**, 097106. [[CrossRef](#)]
40. Vosteen, H.-D.; Schellschmidt, R. Influence of temperature on thermal conductivity, thermal capacity and thermal diffusivity for different types of rock. *Phys. Chem. Earth* **2003**, *28*, 499–509. [[CrossRef](#)]
41. Abootalebi, R.; Siemens, G. Thermal properties of engineered barriers for a Canadian deep geological repository. *Can. Geotech. J.* **2018**, *55*, 759–776. [[CrossRef](#)]
42. Pruess, K.; Oldenburg, C.; Moridis, G. *TOUGH2 User's Guide, Version 2.1*; LBNL-43134; Lawrence Berkeley National Laboratory: Berkeley, CA, USA, 2012.
43. Wagner, W.; Pruß, A. The IAPWS formulation 1995 for the thermodynamic properties of ordinary water substance for general and scientific use. *J. Phys. Chem. Ref. Data* **2002**, *31*, 387. [[CrossRef](#)]
44. Finsterle, S.; Commer, M.; Edmiston, J.; Jung, Y.; Kowalsky, M.B.; Pau, G.S.H.; Wainwright, H.M.; Zhang, Y. iTOUGH2: A simulation-optimization framework for analyzing multiphysics subsurface systems. *Comput. Geosci.* **2017**, *108*, 8–20. [[CrossRef](#)]
45. Saltelli, A.; Ratto, M.; Andres, T.; Campolongo, F.; Cariboni, J.; Gatelli, D.; Saisana, M.; Tarantola, S. *Global Sensitivity Analysis, the Primer*; John Wiley & Sons Ltd.: West Sussex, UK, 2008; p. 292, ISBN 978-0-470-05997-5.

46. Morris, M.D. Factorial sampling plans for preliminary computational experiments. *Technometrics* **1991**, *33*, 161–174. [[CrossRef](#)]
47. Finsterle, S. Practical notes on local data-worth analysis. *Water Resour. Res.* **2015**, *51*, 9904–9924. [[CrossRef](#)]
48. Hurtig, E.; Großwig, S.; Jobmann, M.; Kühn, K.; Marschall, P. Fibre-optic temperature measurements in shallow boreholes: Experimental application for fluid logging. *Geothermics* **1994**, *23*, 355–364. [[CrossRef](#)]
49. Freifeld, B.M.; Finsterle, S.; Onstott, T.C.; Toole, T.; Pratt, L.M. Ground surface temperature reconstructions: Using in situ estimates for thermal conductivity acquired with a fiber-optic distributed thermal perturbation sensor. *Geophys. Res. Lett.* **2008**, *35*, L14309. [[CrossRef](#)]



© 2019 by the authors. Licensee MDPI, Basel, Switzerland. This article is an open access article distributed under the terms and conditions of the Creative Commons Attribution (CC BY) license (<http://creativecommons.org/licenses/by/4.0/>).